ERRATUM

Chapter 46
Modeling of Potential Landslide Tsunami Hazards Off Western Thailand (Andaman Sea)

Julia Schwab, Sebastian Krastel, Mohammad Heidarzadeh, and Sascha Brune

S. Krastel et al. (eds.), *Submarine Mass Movements and Their Consequences*, Advances in Natural and Technological Hazards Research 37, DOI 10.1007/978-3-319-00972-8,

DOI 10.1007/978-3-319-00972-8_62

Abstract We model several scenarios of potential submarine landslide tsunamis in the Andaman Sea off the Thai west coast. Our results suggest that landslides may be capable of producing significant tsunamis. Two categories of submarine landslide scenarios were evaluated. Geometry parameters of the first category are taken from identified mass transport deposits (MTDs); the second category considers a potentially unstable block identified in seismic data. Our preliminary modeling approach shows, that run-up values may reach significant tsunami heights for some scenarios. We point out that our results have to be regarded as only preliminary due to several limitations in our modeling approach. Our results, however, show the need for more sophisticated modeling of landslide tsunamis, especially regarding the failure process and inundation on dry land.

Unfortunately this chapter was published without authors' corrections. The revised version is published as Erratum.

J. Schwab (✉)
Helmholtz Centre for Ocean Research, GEOMAR, Kiel, Germany
e-mail: jschwab@geomar.de

S. Krastel
Institute of Geosciences, Christian-Albrechts-Universität zu Kiel, Kiel, Germany

M. Heidarzadeh
Cluster of Excellence "The Future Ocean", Institute of Geosciences, Christian-Albrechts Universität zu Kiel, Kiel, Germany

S. Brune
GFZ German Research Centre for Geosciences, Potsdam, Germany

The online version of the original chapter can be found at
http://dx.doi.org/10.1007/978-3-319-00972-8_46

46.1 Introduction

Due to its vicinity to the highly seismic Sunda Trench, the Thai west coast is vulnerable to tectonic tsunamis (e.g. Jankaew et al. 2008). Earthquakes, however, are not the only source of tsunami waves. Seismically triggered submarine slope failures are also known for producing large wave heights in the near field (Synolakis et al. 2002). However, tsunami warning is problematic, as landslides may initiate within minutes or hours of an earthquake (e.g. Fritz et al. 2012), and a seismic signal may not even be detectable prior to a landslide.

Schwab et al. (2012) identified several MTDs and indicators for potential future failures at the western edge of Mergui Ridge, which forms a part of the outer Thai shelf. By minimum volume estimations and submergence depth of identified deposits, they concluded that only a few slope failures may have been tsunamigenic, resulting in a low estimate for landslide tsunami hazards. In order to obtain a more detailed picture of the tsunamigenic potential that may arise from these slope failures, this study aims to quantitatively understand the landslide tsunami hazards off western Thailand by numerical modeling.

46.2 Geological Background

Schwab et al. (2012) examined 2D reflection seismic profiles across the Mergui Ridge-East Andaman Basin transition (Fig. 46.1a), and high resolution bathymetric data from the top of Mergui Ridge. They identified several stacked MTDs west of Mergui Ridge (Figs. 46.1b and 46.2a) indicating recurrent slope failures. Based on the thickness of undisturbed sediment packages between individual MTDs, long time intervals (hundreds of kyrs) were estimated between succeeding events. Possible causes for slope failures include ongoing tectonic activity, occurrence of potentially unstable drift deposits and the presence of fluids and resulting overpressure. Additionally, indicators for potential future failures were identified (Fig. 46.2b) at the faulted western edge of Mergui Ridge (Schwab et al. 2012).

46.3 Modeling and Dataset

Based on geometrical parameters derived from seismic and bathymetric dataset (Figs. 46.1b and 46.2), different hypothetical scenarios of landslide tsunami generation were modeled. The dimensions of the modeled slides are comparable to those described by Brune et al. (2010a, b) from neighboring areas. We follow the modeling approach of these authors, which takes into account that small landslides do not fulfill the applicability conditions for more realistic source models (see Brune et al. 2010b for a discussion of the approach). Therefore initial wave heights are calculated by a set of semi-empirical formulas (Watts et al. 2005; Grilli and Watts 2005). These formulas describe the sea surface response to a simplified coherent rotational slump failure. Compared to other more realistic landslide formulas

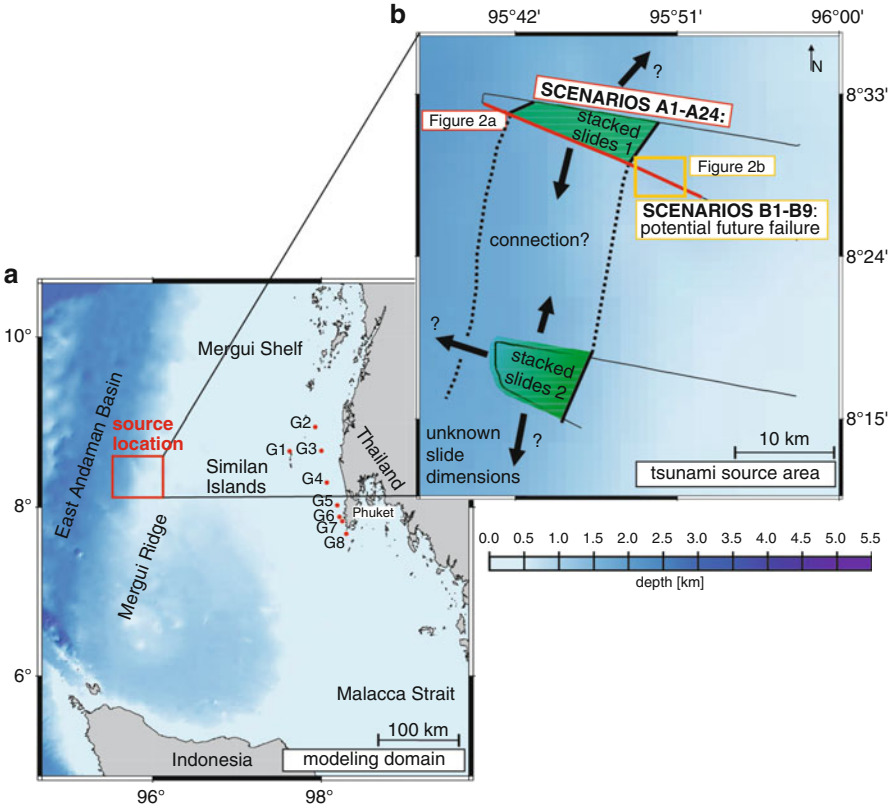

Fig. 46.1 (**a**) Bathymetric map of modeling domain and main structural features. G1–G8 indicate "artificial gauge stations" near the coast (20–50 m water depth) where maximum wave heights of tsunami are derived from. (**b**) Source location for chosen scenarios. *Green* areas indicate the locations where stacked slides have been identified in the basin on seismic profiles (*thin black lines*). *Black arrows* indicate the uncertainty in slide width

(e.g. Mohammed and Fritz 2012) they do not account for the deformation of the slide during the failure process. For calculating tsunami propagation, the TUNAMI-N2 numerical code (e.g. Goto et al. 1997) was applied, and an extension of this code (Brune et al. 2010b) was used to test stability conditions of input parameters and to calculate initial wave heights as described above. The simulations were performed for a total time of 25,200 s for all scenarios with a time step of 0.5 s using the GEBCO bathymetric grid (IOC et al. 2003) resolved to 32 arc sec.

Calculated maximum wave heights are regarded at eight artificial gauge stations G1–G8 (Fig. 46.1a, Table 46.1) placed offshore at water depths of about 20 m (G1) and about 50 m (G2–G8). Empirical formulas were applied to obtain a first estimate of potential run-up heights R1 (Ward and Asphaug 2003) and R2 (Ward and Day 2008) from the maximum offshore wave heights at G1–G8. R1 depends only on water depth and tsunami wave height at an offshore location, whereas for R2 also the slope angle between offshore location and shore line is included.

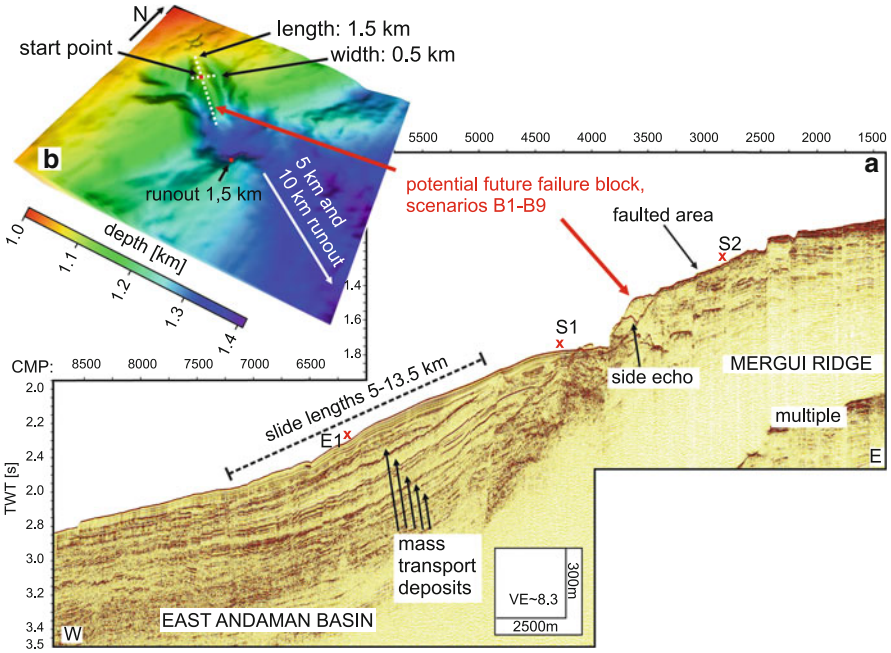

Fig. 46.2 (**a**) 2D reflection seismic profiles across the two source areas, "stacked slides location" and "potentially unstable block". *S1*: start point for slides of scenarios A1–A12, *S2*: start point for slides of scenarios A13–A24. *E1*: Endpoint for slides of scenarios A13–A24. (**b**) Bathymetry of the "potentially unstable block" (scenarios B1–B9). *CMP* Common Midpoint (See Fig. 46.1b for locations)

Table 46.1 Artificial gauge stations

Gauge	G1	G2	G3	G4	G5	G6	G7	G8
Lat [°]	8.6636	8.8639	8.6405	8.2704	8.011	7.8888	7.8404	7.7609
Long [°]	97.6254	98.2577	98.2286	98.27	98.2853	98.2524	98.284	98.3228
Water depth [m]	24	49	50	49	51	48	46	48
Coastal location	Similan Islands	Bang Muang	Khue-kakk	Khok Kloe	Chueng Tao	Patong	Karon	Rawai

46.3.1 Modeled Scenarios

We chose two source locations based on information derived from seismic and bathymetric data (Fig. 46.1). Scenarios A1–A24 correspond to a location of previously-identified, stacked MTDs. Scenarios B1–B9 consider a potentially unstable block (Fig. 46.2, Schwab et al. 2012).

46.3.1.1 Scenarios A1–A24, "Stacked Slides Location"

The "stacked slides location" is situated west of the Mergui Ridge (Fig. 46.1b). Four parallel seismic reflection profiles show a similar pattern of five stacked MTDs (Fig. 46.2a). Geometrical properties of the modeled slides were varied according to the dimensions of identified slides with lengths between 5 and 13.5 km. Widths of 5, 7 and 30 km were chosen, the latter width value assuming that the two areas of stacked MTDs are connected, while the smaller values imply separate failure events. The slide thickness applied for these scenarios was 150 m, which is the maximum thickness measured for all detected MTDs. We use slope angles of 3° and 6°, corresponding to the range of slope angles in the source area. The origin of the MTDs is unknown, therefore we assume two different locations for slide initiation at the edge of the ridge in about 880 m water depth (run-out distance 15.5 km) and at the upper boundary of the basin in about 1,270 m water depth (run-out distance 7.5 km, Fig. 46.2a).

46.3.1.2 Scenarios B1–B9: "Potentially Unstable Block"

In scenarios B1–B9, we model the failure of a potentially unstable sedimentary block located at the edge of Mergui Ridge in about 1,100 m water depth (Fig. 46.2a) (Schwab et al. 2012). Its dimensions (Table 46.3) are derived from bathymetric data (Fig. 46.2b). Different run-out distances (1.5, 5 and 10 km) and slope angles (3°, 6° and 14.5) were used (Table 46.3).

46.4 Results

Initial positive wave heights (η_{plus}) for scenarios A1–A24 range between 1.5 and 118.1 m (Table 46.2). η_{plus} values larger than 40 m are reached for scenarios with long run-out distances and short slide lengths of 5 km (A13, A15, A17, A19, A21, A23). Arrival times of the first tsunami waves at the coast (32–37 min) are similar for all scenarios. A_{20max}, the maximum offshore wave height at G1, ranges between 1.3 and 22.8 m for the A-scenarios. Run-up estimations from A_{20max} range between 2.3 and 23.1 m (R1) and 8.0 and 25.8 m (R2), respectively.

For scenarios B1–B9, η_{plus} ranges between 1.7 and 28.2 m (Table 46.3). Arrival times are in the same range as for the A-scenarios (37–40 min). Compared to A1–A24, the A_{20max} values of B1–B9 are smaller (0.01–0.24 m). Run-up estimations are in the range of 0.04–0.61 m (R1) and 1.0–4.0 m (R1) respectively.

The maximum wave height distributions strongly depend on slide input parameters (Tables 46.2 and 46.3, Figs. 46.3 and 46.4). Despite its larger length, scenario A2 produces smaller wave heights compared to scenario A1 (Fig. 46.3a, b). Scenario

Table 46.2 Key modeling parameters for scenario A1–A24

Scenario	A1	A2	A3	A4	A5	A6	A7	A8	A9	A10	A11	A12
Runout [km]	7.5	7.5	7.5	7.5	7.5	7.5	7.5	7.5	7.5	7.5	7.5	7.5
SLA [°]	3	3	3	3	3	3	6	6	6	6	6	6
DIM [km × km]	5 × 5	5 × 13.5	7 × 5	7 × 13.5	30 × 5	30 × 13.5	5 × 5	5 × 13.5	7 × 5	7 × 13.5	30 × 5	30 × 13.5
Th [m]	150	150	150	150	150	150	150	150	150	150	150	150
Vol [km^3]	2.9	8.0	4.1	11.1	17.7	47.7	2.9	8.0	4.1	11.1	17.7	47.7
η_{plus} [m]	10.8	1.5	13.2	2.0	23.7	5.0	12.6	1.8	15.5	2.3	27.6	5.8
Ta [min]	36	37	36	36	33	32	36	36	36	36	33	32
A_{20max} [m]	2.3	1.3	3.0	1.8	7.7	5.6	2.6	1.5	3.5	2.1	8.7	6.6
R1 [m]	3.6	2.3	4.6	3.0	9.6	7.5	4.1	2.6	5.1	3.4	10.6	8.5
R2 [m]	10.0	8.0	11.3	9.1	16.5	14.5	10.6	8.5	11.9	9.7	17.4	15.5
Scenario	A13	A14	A15	A16	A17	A18	A19	A20	A21	A22	A23	A24
Runout [km]	15.5	15.5	15.5	15.5	15.5	15.5	15.5	15.5	15.5	15.5	15.5	15.5
SLA [°]	3	3	3	3	3	3	6	6	6	6	6	6
DIM [km × km]	5 × 5	5 × 13.5	7 × 5	7 × 13.5	30 × 5	30 × 13.5	5 × 5	5 × 13.5	7 × 5	7 × 13.5	30 × 5	30 × 13.5
Th [m]	150	150	150	150	150	150	150	150	150	150	150	150
Vol [km^3]	2.9	8.0	4.1	11.1	17.7	47.7	2.9	8.0	4.1	11.1	17.7	47.7
η_{plus} [m]	49.8	6.8	60.4	8.9	101.4	21.0	58.0	8.0	70.3	10.4	118.1	24.4
Ta[min]	36	37	36	36	33	32	36	37	36	36	32	31
A_{20max} [m]	7.3	5.2	9.2	7.1	15.9	20.3	8.2	6.1	10.2	8.3	16.5	22.8
R1 [m]	9.3	7.1	11.2	9.1	17.2	21.0	10.2	8.0	12.1	10.3	17.8	23.1
R2 [m]	16.2	14.1	17.8	16.0	22.2	24.6	17.0	15.0	18.6	17.1	22.6	25.8

SLA local slope angle, *Runout* run-out distance, *DIM* slide dimensions in width × length, *Th* thickness of slide, *Vol.* Volume of the slide, calculated as given in Grilli and Watts (2005), η_{plus} initial wave height, *Ta* arrival time, A_{20max} maximum wave height (surface elevation) at G1, *R1* run-up calculated for A_{20max} after Ward and Asphaug (2003), *R2* run-up calculated after Ward and Day (2008)

Table 46.3 Key modeling parameters for scenarios B1–B9

Scenario	B1	B2	B3	B4	B5	B6	B7	B8	B9
Runout[km]	1.5	5	10	1.5	5	10	1.5	5	10
SLA [°]	3	3	3	6	6	6	14.5	14.5	14.5
DIM [km × km]	0.5 × 1.5	0.5 × 1.5	0.5 × 1.5	0.5 × 1.5	0.5 × 1.5	0.5 × 1.5	0.5 × 1.5	0.5 × 1.5	0.5 × 1.5
Th [m]	125	125	125	125	125	125	125	125	125
Vol [km^3]	0.07	0.07	0.07	0.07	0.07	0.07	0.07	0.07	0.07
η_{plus}[m]	1.7	9.0	24.2	2.0	10.5	28.2	2.4	12.8	34.2
Ta[min]	40	37	37	40	37	37	37	39	40
A_{20max}[m]	0.01	0.06	0.17	0.01	0.070	0.20	0.01	0.09	0.24
R1[m]	0.04	0.20	0.47	0.04	0.23	0.53	0.05	0.27	0.61
R2[m]	1.0	2.3	3.5	1.0	2.4	3.7	1.1	2.7	4.0

SLA local slope angle, *Runout* run-out distance, *DIM* slide dimensions in width × length, *Th* thickness of slide, *Vol.* Volume of the slide, calculated after Grilli and Watts (2005), η_{plus} initial wave height, *Ta* arrival time, A_{20max} maximum wave height (surface elevation) at G1, *R1* run-up calculated for A_{20max} after Ward and Asphaug (2003), *R2*: run-up calculated after Ward and Day (2008)

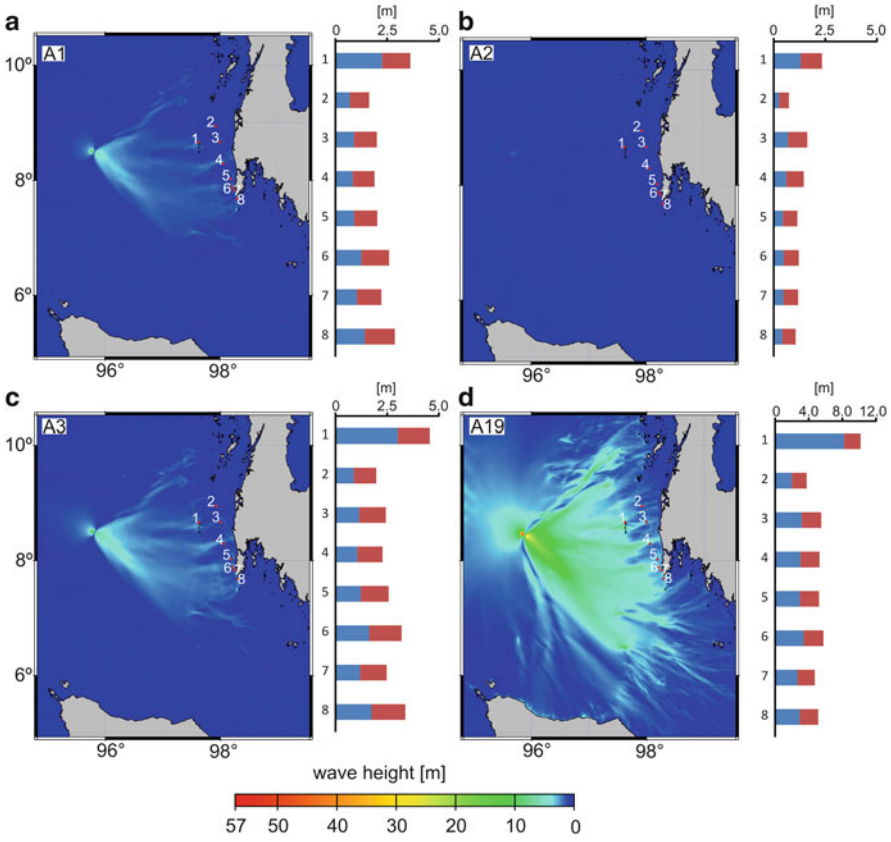

Fig. 46.3 Examples for wave height distributions from hypothetical failures at the "stacked slides location", as well as maximum wave heights (*blue bars*) and R1 run-up estimations (*red bars*) for artificial gauge stations G1–G8. Note the different scales for the wave height/run-up charts

A3 has a larger width compared to A1 and produces larger wave heights. Scenario A19 has the same slide dimensions as A1 but a larger run-out distance and larger slope angle (Fig. 46.3d, Table 46.2). This scenario also results in larger wave heights compared to A1.

Generally, largest maximum wave heights arise near the source area and in a triangular zone towards the coast. Regarding maximum wave heights at individual gauge locations, G1 records the largest run-up estimations (Fig. 46.3).

Figure 46.4 demonstrates the difference in wave heights for different run-out distances and slope angles of the B-scenarios (Table 46.3). Compared to the A-scenarios, the tsunami wave heights are smaller and not focused towards the coast, indicating reduced tsunami potential of the B-scenarios.

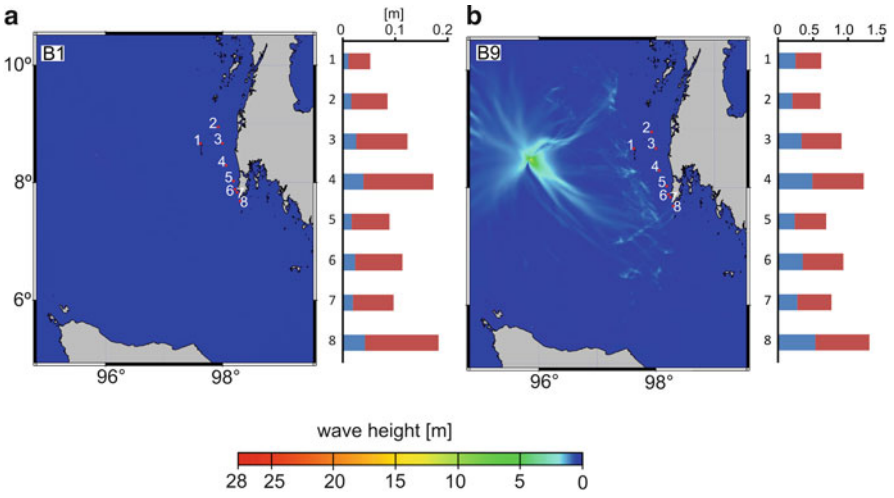

Fig. 46.4 Examples for wave height distributions from hypothetical failures at "potentially unstable block" location, as well as maximum wave heights (*blue bars*) and R1 run-up estimations (*red bars*) for artificial gauge stations G1–G8. Note the different scales for the wave height/run-up charts

46.5 Discussion and Conclusions

Our results give first insights into the tsunamigenic potential of slope failures off western Thailand. These results are only a preliminary assessment of landslide tsunami potential due to the limitations of the chosen approach:

1. The failure process that produced the MTDs in the working area is unknown. Therefore initial wave heights were calculated from failures, modeled as simplified coherent rotational slumps. More realistic failure scenarios such as translational and/or disintegrating slides or in the form of multiple events would produce smaller wave heights (Masson et al. 2006), but were not modeled in our preliminarily approach. Hence our modeled initial wave height is most likely overestimated.
2. In our numerical simulations, wave evolution beyond water depth of 20 m is prohibited, therefore run-up values were estimated by empirical equations using offshore wave heights at only a few isolated points (G1–G8), and inundation modeling was not performed at all. Empirical equations have limitations, the results vary for different equations (Tables 46.2 and 46.3), and near-shore wave phenomena reducing run-ups such as wave breaking are not considered by these empirical formulas.
3. Tsunami propagation was calculated from a coarse bathymetric grid and by shallow-water equations, which do not take into account effects such as dispersion. This may lead to inaccuracy of wave calculations.

4. The dimensions of the landslides in the A-scenarios are inferred from MTDs, as the pre-failure dimensions of the slides are not known. Thereby a thickness of 150 m was chosen for all scenarios, as thickness is the least determined value based on our seismic field data. This means that, as thickness is an important factor for wave generation, the calculation of initial wave height may contain inaccuracies.
5. The seismic images of the MTDs show clear signs of disintegration. This means that deformation occurred during the failure. According to Mohammed and Fritz (2012) deformation during the failure process leads to energy conversion and hence wave reduction. This again suggests that wave heights calculated in this study may be overestimated.

Landslide tsunamis are often described as a local phenomenon with large run-up heights limited to the near-field (Synolakis et al. 2002). Our results for the A-scenarios show such patterns (Fig. 46.3d), with a triangular zone of large maximum wave heights, presumably indicating a delimited area where tsunami hazard may occur at the coast. Some of the scenarios studied here show potential tsunami hazards comparable to the Papua New Guinea landslide tsunami of July 1998, where large run-up heights of more than 10 m were observed on a very limited coastline of about 20 km (Synolakis et al. 2002). A location especially exposed to a tsunami would then be around the gauge station G1, where the largest run-up heights were estimated.

Contrasting to the modeling results of A1–A24, the B-scenarios produce lower run-up height estimations, which are reasonable due to their smaller landslide volume and more realistic slide dimensions, and which are comparable to values described by Jintasaeranee et al. (2012).

Our results suggest that a landslide tsunami hazard for the coastal areas may exist, and wave heights and run-up estimations may increase with slope angle, run-out distance and slide volume. The width/length ratio of the slides is also affecting our preliminary results, as in most cases an increase in length leads to unexpected decrease in wave heights. This finding has to be examined in greater detail in the future.

Unlike tectonic tsunamis, landslide tsunami sources cannot not be located based on global networks and they may be located close to the shoreline (e.g. Fritz et al. 2012). Therefore landslide tsunamis are almost unpredictable making tsunami warning impossible. Short arrival times of around 30 min or less are typical for near-field tsunamis. The calculated arrival times of our model scenarios are close to this range, indicating that warning time for coastal areas would be short, adding to the unpredictability of landslide tsunamis.

Because of the previously mentioned limitations of our model approach, our results only represent worst case scenarios. This is especially true for the A-scenarios with largest volumes. Furthermore, recurrence rates for major tsunamigenic earthquakes in the area are estimated by 400 years (Monecke et al. 2008), whereas landslide recurrence is estimated to be in the range of 100 kyrs (Schwab et al. 2012). Hence, landslide tsunamis do not represent a major additional risk for the Thai coast.

However, they cannot be neglected and we recommend further geological surveys in the region to better locate sizes and distribution of submarine landslides, and sophisticated numerical modeling in order to reliably assess their hazard potential.

Acknowledgments The TUNAMI-N2 code is originally authored by Fumihiku Imamura and Nobou Shuto and copyrighted to Ahmet C. Yalciner, Fumihiku Imamura and Costas E. Synolakis. We acknowledge them for developing and making available the code. We thank the reviewers Hermann Fritz and Marc de Batist for their careful reviews and constructive comments that helped to improve the manuscript.

References

Brune S, Babeyko AY, Ladage S, Sobolev SV (2010a) Landslide tsunami hazard in the Indonesian Sunda Arc. Nat Hazards Earth Sys 10:589–604. doi:10.5194/nhess-10-589-2010

Brune S, Ladage S, Babeyko AY et al (2010b) Submarine landslides at the eastern Sunda margin: observations and tsunami impact assessment. Nat Hazards 54:547–562. doi:10.1007/s11069-009-9487-8

Fritz HM, Hillaire JV, Molière E, Wei E, Mohammed F (2012) Twin tsunamis triggered by the 12 January 2010 Haiti earthquake. Pure Appl Geophys. doi:10.1007/s00024-012-0479-3

Goto C, Ogawa Y, Shuto N, Imamura F (1997) IUGG/IOC TIME Project: Numerical method of tsunami simulation with the leap-frog scheme. In Intergovernmental Oceanographic Commission, manuals and guides no. 35, UNESCO

Grilli ST, Watts P (2005) Tsunami generation by submarine mass failure. Part I: modeling, experimental validation, and sensitivity analysis. Waterw Port C-ASCE 131(6):283–297

IOC, IHO, BODC (2003) Centenary edition of the GEBCO digital atlas, published on CD-ROM on behalf of the Intergovernmental Oceanographic Commission and the International Hydrographic Organization as part of the general bathymetric chart of the oceans. British oceanographic data centre, Liverpool

Jankaew K, Atwater BF, Sawai Y et al (2008) Medieval forewarning of the 2004 Indian Ocean tsunami in Thailand. Nature 455:1228–1231. doi:10.1038/nature07373

Jintasaeranee P, Weinrebe W, Klaucke I et al (2012) Morphology of the Andaman outer shelf and upper slope of the Thai exclusive economic zone. J Asian Earth Sci 46:78–85

Masson DG, Harbitz CB, Wynn RB et al (2006) Submarine landslides: processes, triggers and hazard prediction. Philos Trans R Soc A 364:2009–2039

Mohammed F, Fritz HM (2012) Physical modeling of tsunamis generated by three-dimensional deformable granular landslides. J Geophys Res 117(C11):C11015

Monecke K, Finger W, Klarer D et al (2008) A 1,000-year sediment record of tsunami recurrence in northern Sumatra. Nature 455:1232–1234. doi:10.1038/nature07374

Schwab JM, Krastel S, Grün M et al (2012) Submarine mass wasting and associated tsunami risk offshore western Thailand, Andaman Sea, Indian Ocean. Nat Hazards Earth Sys 12:609–2630. doi:10.5194/nhess-12-2609-2012

Synolakis CE, Bardet J-P, Borrero JC et al (2002) The slump origin of the 1998 Papua New Guinea tsunami. Proc R Soc Lond A 458:763–789

Ward SN, Asphaug E (2003) Asteroid impact tsunami of 2880 March 16. Geophys J Int 153:F6–F10. doi:10.1046/j.1365-246X.2003.01944.x

Ward SN, Day S (2008) Tsunami balls: a granular approach to tsunami runup and inundation. Commun Comput Phys 3(1):222–249

Watts P, Grilli ST, Tappin D, Fryer GJ (2005) Tsunami generation by submarine mass failure. Part II: predictive equations and case studies. Waterw Port C-ASCE 131(6):298–310